SOFT ROBOTS

Electronic skins for soft, compact, reversible assembly of wirelessly activated fully soft robots

Junghwan Byun,[1,2,3]* Yoontaek Lee,[1]* Jaeyoung Yoon,[1] Byeongmoon Lee,[1] Eunho Oh,[1] Seungjun Chung,[4] Takhee Lee,[5] Kyu-Jin Cho,[2,3]† Jaeha Kim,[1]† Yongtaek Hong[1]†

Designing softness into robots holds great potential for augmenting robotic compliance in dynamic, unstructured environments. However, despite the body's softness, existing models mostly carry inherent hardness in their driving parts, such as pressure-regulating components and rigid circuit boards. This compliance gap can frequently interfere with the robot motion and makes soft robotic design dependent on rigid assembly of each robot component. We present a skin-like electronic system that enables a class of wirelessly activated fully soft robots whose driving part can be softly, compactly, and reversibly assembled. The proposed system consists of two-part electronic skins (e-skins) that are designed to perform wireless communication of the robot control signal, namely, "wireless inter-skin communication," for untethered, reversible assembly of driving capability. The physical design of each e-skin features minimized inherent hardness in terms of thickness (<1 millimeter), weight (~0.8 gram), and fragmented circuit configuration. The developed e-skin pair can be softly integrated into separate soft body frames (robot and human), wirelessly interact with each other, and then activate and control the robot. The e-skin–integrated robotic design is highly compact and shows that the embedded e-skin can equally share the fine soft motions of the robot frame. Our results also highlight the effectiveness of the wireless inter-skin communication in providing universality for robotic actuation based on reversible assembly.

INTRODUCTION

Body compliance is a salient feature of robots that perform mechanical work in dynamic, unstructured environments. By designing softness into each robot part (body frame, actuator, sensor, etc.), a recent stream of research on robotics has aimed for organically integrating component parts without rigid boundaries that often interfere with dynamic environments or soft continuum motions of the robot itself (*1*, *2*). This inherent compliance of soft robots extends the functionality of robots toward intimate interaction with humans (*3*), in-depth interpretation of biological models (*4*–*9*), and biomedical applications (*10*, *11*). In this regard, many efforts have been made to develop a combinatorial soft body architecture in which soft actuators or actuating architectures such as tendon cables (*12*–*14*), pneumatic networks (*7*, *15*–*17*), and electroactive polymers (*8*, *18*) are integrated into a soft body frame.

Although the compliance match between this body architecture and surrounding environment has successfully been achieved in most soft robotic applications, physical layouts of a driving system—composed of actuating drivers (e.g., pressure-regulating components), electronic control circuits and communication boards (printed circuit boards), and sensors—still rely on rigid components. Hence, entire robotic systems are found to be partially hard and can themselves interfere with soft continuum motion. To minimize the effect of this compliance gap on robot function, practical soft robots have required physically isolated spaces for equipping hard components, the location and structure of which should not obstruct the motion and function of the robots: Representative examples include rigid support fixtures and frames for soft robotic hands or grippers (*3*, *19*–*22*), flying robots (*6*), internal spaces of robot bodies for self-contained soft crawling or swimming robots (*7*, *8*, *18*), and dorsal containers for soft mobile or jumping robots (*23*–*25*). However, this rigid assembly with additional structures that need to be designed in the stationary (or inactive) parts inevitably define rigid boundaries in a soft frame and also incur the issues of weight, volume, and design cost. Furthermore, some robotic applications that address thin, compact body frames (thus, there is not enough space to accommodate the isolated driving system) essentially need alternative layouts of driving systems. Reflecting these limitations, a few recent studies have made a first step in designing softness into a driving part based on nontraditional approaches such as three-dimensional (3D) printed microfluidic logics (*26*) and replicated optogenetic tissue design (*27*).

We propose a skin-like soft driving system based on soft electronics for the implementation of fully soft robot. Soft electronics is a class of electronic systems that integrate devices and/or circuits onto a soft substrate for intimate interfacing with biological or unpredictable curvilinear surfaces (*28*). Because of the compliance match between the electronic platform and natural organism, electronic functionalities such as sensory transduction (*29*–*32*), biological stimulation (*33*), and computation (*34*, *35*) can be implanted into the target soft tissues as an "electronic skin (e-skin)." Recently, assemblies of hard integrated circuit (IC) devices, rather than thin-film devices, into a soft platform have taken soft electronics one step further with the capability of "in-skin" computation—namely, stretchable hybrid electronics (SHE) (*34*–*39*). Promising studies in this direction include transfer-combined microfluidic assembly (*36*), modified flip-chip bonding (*37*), 3D microstructure design (*38*), and printing-based assembly (*34*, *35*, *39*). Given the abilities to not only match the compliance with the robot body but also integrate high-performance electronic functionality, it is promising that this SHE design can play an important role as a driving core of soft robots (*1*, *40*). However, the existing methodologies are too complicated to be practical for demonstrating robot function. Furthermore, the

[1]Department of Electrical and Computer Engineering, Inter-University Semiconductor Research Center, Seoul National University, Seoul, Republic of Korea. [2]Department of Mechanical and Aerospace Engineering, Institute of Advanced Machines and Design, Seoul National University, Seoul, Republic of Korea. [3]Soft Robotics Research Center, Seoul National University, Seoul, Republic of Korea. [4]Photoelectronic Hybrids Research Center, Korea Institute of Science and Technology, Seoul, Republic of Korea. [5]Department of Physics and Astronomy, Seoul National University, Seoul, Republic of Korea.
*These authors contributed equally to this work.
†Corresponding author. Email: yongtaek@snu.ac.kr (Y.H.); jaeha@snu.ac.kr (J.K.); kjcho@snu.ac.kr (K.-J.C.)

lumpy system configurations (dimension of embedded IC components, >10 mm by 10 mm) that most approaches have used to interface with typical parts of the human body—such as a wrist, arm, forehead, and chest (bending radius, >10 to 20 mm) (*36*–*39*, *41*, *42*)—cannot meet the design requirement of soft robots that frequently deform into much larger curvature.

Here, we present an e-skin pair as a two-part soft driving system whose physical layout and electronic functionality enables soft, compact, and reversible assembly of driving capability into the soft robot frame for a previously unknown direction of fully soft robotic design (Fig. 1A). The proposed e-skin design is soft (same material for the body architecture), thin (<1 mm), and lightweight (~0.8 g) and features the spatially fragmented SHE configuration with a slew of miniature IC components (standard dimension, <1.5 mm by 1.5 mm). This unique design minimized the local inherent hardness arising from chip-scale components and thus allowed the e-skins to be softly and compactly integrated into soft body frames (robot and human). According to each function, we term the e-skin at the robot side as an activating e-skin (Fig. 1B) and that at the human side as a controlling e-skin (Fig. 1C). For electronic functionality, the e-skin pair was designed to perform wireless communication of the four-state control signal, namely, "wireless inter-skin communication," and to activate the robot when mounted onto each soft body (human and robot). The reliability of the wireless inter-skin communication is validated by a sufficient level of tolerance to both mechanical (bending, stretching, and folding) and electrical (environmental noise) stresses. To show the benefits of this concept, we demonstrated an integrated design of a thin, compact, and fully soft robotic hand driven by e-skin–mediated wireless activation. In this robotic design, soft actuators and e-skin were compactly assembled into a soft body frame without incurring the inherent hardness, so that the deformation profile of the robot could be equally shared with every robot part (Fig. 1B). This coadaptive movement helped the robot pass through and/or operate in highly confined spaces, whose cross section was even smaller than robot size. We further showed that the presented e-skin pair and corresponding wireless inter-skin communication concept can be an attractive method for untethered, multirobot activation regardless of body architectures and their deformation states, realizing universal soft robotic activation.

RESULTS

Fragmented SHE design for fine conformability

The e-skins were designed in a way that maximized their compliance to fine continuous motions of soft body frames. The key point for this design requirement is twofold: (i) in an electrical viewpoint, to eliminate the lumpy and excessive functions (e.g., bulky IC processors and Bluetooth boards) and instead to devise the compact circuit architecture for four-state wireless robot control (see fig. S1 for the customized circuit architecture); and (ii) in a physical viewpoint, to spatially distribute this circuit architecture with a slew of miniature IC components to minimize the inherent hardness arising from chip-scale components (fig. S2 for fragmentation). Although such design criteria required complex soft networks between numerous surface-mountable devices (SMDs), we solved this issue by using a fully printable SMD assembly technique (see Materials and Methods and figs. S3 and S4) (*34*, *35*). This printing-based approach allowed us to define proper circuit architectures in a more rapid and flexible manner through a mask-free, continuous fabrication process, compared to other existing approaches that generally require multistep masking processes (*36*–*38*).

The fabricated e-skin pair consisted of more than 80 SMDs (~50 ICs, ~30 passive components, antenna, etc.) based on four functional layers:

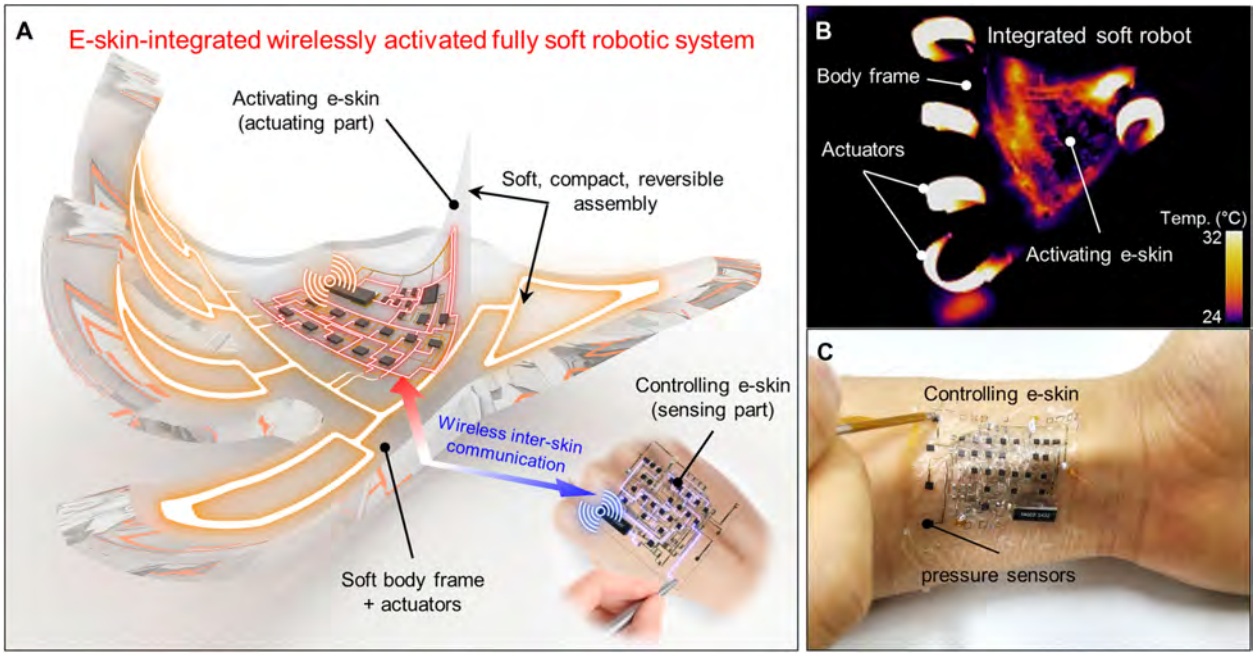

Fig. 1. Skin-like soft driving system for wirelessly activated fully soft robots. (**A**) Conceptual illustration of e-skin–mediated soft robotic assembly and wireless activation. The e-skin pair can be softly, compactly, and reversibly assembled into separate soft body frames (robot and human); wirelessly interact with each other; and then activate and control the robot, realizing fully soft robots. (**B**) Activating and operating behavior of the integrated soft robot visualized by thermographic mapping. In this design, dynamic actuation profiles can be shared with every robot part. (**C**) The embedded controlling e-skin that interacts with human for user-interactive pressure sensing.

SMDs, printed epoxies (Ag epoxy and epoxy), printed multilayer stretchable interconnects (Ag), and a soft foundation [poly(dimethyl siloxane) (PDMS)] (see Fig. 2A, figs. S4 to S6, and table S1 for SMDs and printed multilayer stretchable interconnection networks). Compared to our previous approach (*34*, *35*), we exploited the geometric design of printed epoxy structures for rapid, reliable SMD assembly that effectively preserved the contact area from mechanical stresses without the need for embedded island structures (inset images of Fig. 2A and figs. S7 to S9; see also note S1 for details on the effect of the epoxy structures). The overall layouts of the e-skin pair revealed that electronic functionalities for soft driving system—such as sensors, electronic control circuit and communication board, and actuating drivers—were fragmented into the two-part e-skin system for wireless activation (Fig. 2B).

One of the key design requirements for the e-skins to share the large bending curvature ($1/r$), which could be the deformation profile of soft robots, was to regulate the size (side length, a; thickness, t) and pitch (p) of the assembled SMDs. On the basis of the analytic design criteria described in fig. S10 and note S2, a sufficient condition of design parameters for target r_{min}, dominantly determined by the inward bending state, can be expressed as $r_{min} = \sqrt{a^2/2 + at + t^2}$, $p_{min} = a + 2r_{min}(\pi/4 - \sin^{-1}(a/2r_{min}))$. Given these formulas, we designed the fragmented circuit configuration with the standard SMD dimensions (≤1.5 mm by 1.5 mm by 0.6 mm) and engineered pitch (≥2.3 mm) to satisfy the target deformation curvature ($1/r_{min} \approx 1/1.5\ mm^{-1}$) (Fig. 2C). The resulting e-skin can be stretched and conformed onto the dynamic surface like human skin (fig. S11). Further extreme compliance was showcased by the delicate sharing of the corrugated surface with multiple curvatures (Fig. 2D).

Wireless four-state inter-skin communication

Figure 3A shows the devised circuit architecture for wireless inter-skin communication with four-state robot control signals. According to the function, each e-skin was separately defined: (i) the controlling e-skin that interacted with human for sensing and (ii) the activating e-skin that interacted with a soft robot body for activation. The detailed role of the controlling e-skin was to receive four-state input information (A to D) from user-interactive pressure sensing, encode the input

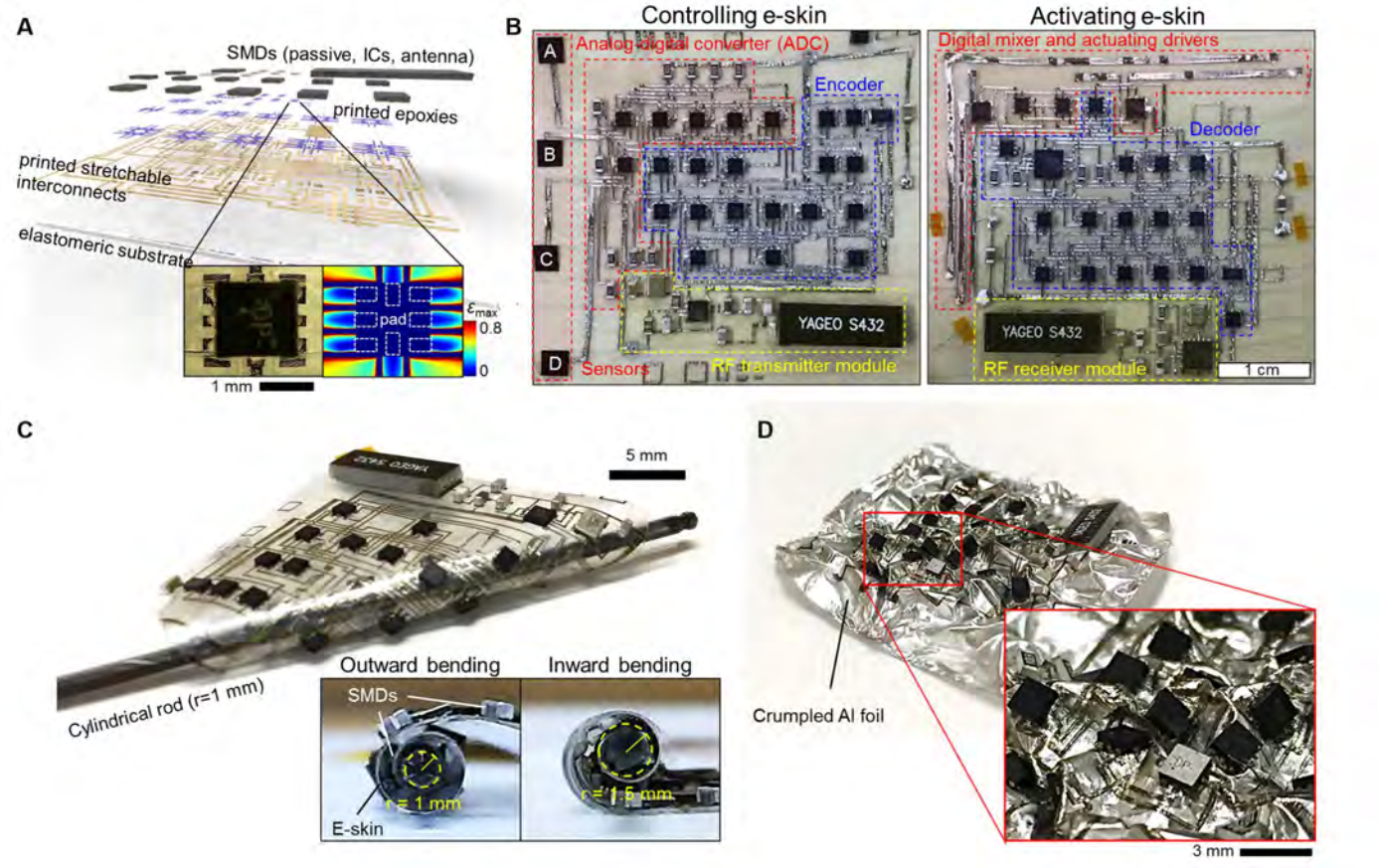

Fig. 2. Fragmented SHE design of e-skins for fine conformability. (**A**) Exploded view schematic illustration of e-skins. Inset images: Optical image (left) and corresponding surface strain field (right), evaluated by finite element analysis, of the unit SMD region. (**B**) Layout and functional description of the e-skin pair: controlling e-skin (left) and activating e-skin (right). Electronic functionalities for soft driving system, such as sensors, electronic control circuit and communication board, and actuating drivers, are spatially fragmented into two parts, providing wireless driving capability. (**C**) Photograph of the e-skin that wraps around the cylindrical rod (radius = 1 mm). The fragmented circuit configuration with the standard SMD dimensions (≤1.5 mm by 1.5 mm by 0.6 mm), and engineered pitch (≥2.3 mm) achieved the target deformation curvature ($1/1.5\ mm^{-1}$) in both outward and inward bending states (inset images) (see fig. S10 and note S1 for details on design criteria). (**D**) Extreme compliance of the e-skin that conforms to the corrugated surface (Al foil) with multiple curvatures.

sequence, and wirelessly transmit it; that of the activating e-skin was to receive and decode it and last activate a soft robot (see figs. S12 to S14 and note S3 for details on the signal flow). When designing this compact circuit architecture instead of adopting lumped ICs or commercially available bulky modules, we used a digital-type signal modulation technique [amplitude shift keying (ASK) modulation] (*43*)

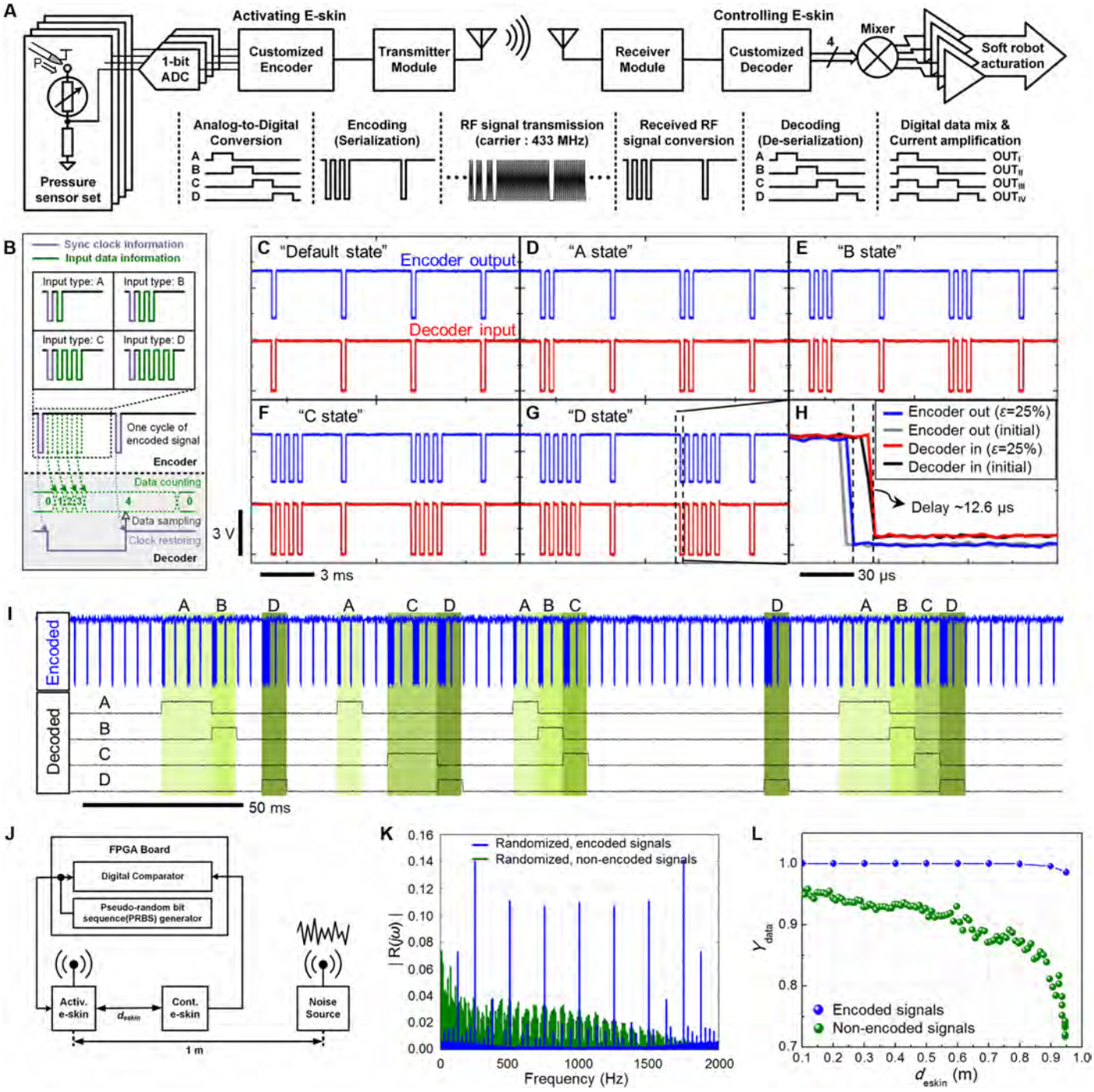

Fig. 3. Wireless four-state inter-skin communication. (**A**) Schematic diagram and representative signal profiles of the devised circuit architecture. (**B**) Encoding/decoding mechanism of the customized serializing encoder/deserializing decoder. (**C** to **G**) Typical encoded waveforms in each input state (default, A to D) measured at the encoder output (before transmitting, blue line) and decoder input (after receiving, red line). (**H**) Magnified view in the waveform in (G). Wireless synchronization between the e-skins within the margin of communication delay of ~12.6 μs was confirmed without meaningful degradation under 25% biaxial strain. (**I**) Real-time decoding process of the dynamic, randomly encoded signal sequences. The decoding capability shows real-time synchronized sampling with the minimum decoding resolution of ~8 ms. (**J**) Schematic illustration of an experimental setup for testing the reliability of the wireless inter-skin communication under artificial noise condition. (**K**) Fourier analysis data on randomized, encoded (blue) and nonencoded (green) signals (typical waveforms are described in fig. S16C). $R(j\omega)$ is defined as the Fourier-transformed pseudo-random bit sequence signals. (**L**) Wireless data transmission yield (Y_{data}) of encoded and nonencoded signals as a function of d_{eskin} defined in (J).

with customized encoding/decoding mechanism. Especially, several circuitry technologies were used to enable "in-circuit" compensation for the stretch/noise-induced partial signal degradation in addition to geometric effects described in figs. S6 to S9.

The specific data encoding/decoding principle is described in Fig. 3B. The key idea is to simultaneously transmit input data and synchronized clock in the form of 1-bit serialized digital signal sequences for wireless synchronization between physically separate e-skins, distinct from a typical source-synchronous interface that relies on separate 2-bit signals for data transmission (Fig. 3B, top) (*44*). Specifically, the input data information was encoded into the number of negative edges (total of five states—1, default; 2, A; 3, B; 4, C; and 5, D), and the clock information was represented by the periodic negative pulses [128 Hz = 1/16 × system clock (2048 Hz)]. Because the clock information was involved in the transmitted signal, the receiver part (activating e-skin) could restore the clock—identical to that of the controlling e-skin—and decode the signal through accurate data sampling without timing mismatch (Fig. 3B, bottom). That is, the e-skin pair was wirelessly synchronized by communicating the clock information.

To show the validity of our encoding mechanism, we measured the encoded signals in each input state at both the encoder output (before transmitting, blue line) and decoder input (after receiving, red line) [see Fig. 3, C to G, and fig. S13 for continuous monitoring (20 s)]. From the results, the devised encoder accurately constructed the serialized data sequence and realized wireless synchronization between the e-skin pair. The magnified profiles of each encoded waveform verified the stretch-tolerant in-skin reliability of both e-skins (25% biaxial strain), and the effective communication delay was found to be ~12.6 μs (~0.16% of the synchronized clock period) (Fig. 3H). The synchronized data sampling and corresponding decoding capability of the activating e-skin were validated by successful decoding responses of 4-bit signals (minimum resolution, ~8 ms) to dynamic sequences of the randomly encoded signal (Fig. 3I).

Reliability under artificial noise condition

The presented encoding mechanism also contributed to the noise-tolerant feature of the wireless inter-skin communication. Inherently, the transmission accuracy of ASK modulation is prone to be degraded by noise signals when the amplitude threshold of the receiver is not settled on a proper level (*45*). Our design strategy of periodically switching the signal bit even in a default state (refer to Fig. 3C) neatly resolved this issue by supporting the threshold optimization. The tolerance of the encoding mechanism to electrical stress was investigated by comparing the wireless data transmission yield (Y_{data}) between the encoded and nonencoded signals under the artificial noise environment. The experimental setup was composed of the e-skin pair (either involving the encoder/decoder or not), a field-programmable gate array (FPGA) board, and a noise source [a radio-frequency (RF) transmitter module connected to a function generator (AFG3102C, Tektronix)] (Fig. 3J; see also figs. S15 and S16 and note S4 for details on the experimental setup). Figure S16C shows the typical waveforms of the randomly generated encoded (blue) and nonencoded (green) signals: The encoded waveform showed well-regulated periodic sequences even in a default state (Fig. 3C), but the nonencoded one was normally "0" in a default state (no input case). The difference in this default periodicity led to the different profiles of frequency components in the result of Fourier analysis, where the encoded signal was composed of the fundamental frequency of 256 Hz (the periodic frequency of negative edges) and its harmonic frequencies but the nonencoded one was not regulated (Fig. 3K). Given these typical waveforms, Y_{data} was explored as a function of the distance between the e-skin pair (d_{eskin} = 0.1 to 0.95 m) (Fig. 3L). The result showed that the encoded periodicity helped the amplitude threshold settle at an optimal level and made the system tolerant to harsh noise condition (the minimum Y_{data} was ~98.63% measured at d_{eskin} = 0.95 m, the nearest region to a noise source). On the other hand, Y_{data} of the nonencoded data suffered an initial degradation (Y_{data} ~95% at d_{eskin} = 0.01 m) and was markedly exacerbated as d_{eskin} increased (Y_{data} ~70% at d_{eskin} = 0.95 m).

E-skin–mediated assembly and wireless activation of a soft robotic hand

Attractive features of the e-skin pair in terms of softness, light weight, and wireless electronic functionality can lead to design of soft robots that are fully compliant in every part and can be wirelessly activated. To showcase the benefits of this skin-type soft driving system, we demonstrated a thin (total thickness, <2 mm), compact, soft robotic hand whose body dimensions could not possibly equip any other types of conventional driving systems. Figure 4A shows soft, compact assembly of actuators and driving system (activating e-skin) for the integrated design of the fully soft robotic hand. A body architecture of this robot was formed by printing poly(3,4-ethylenedioxythiophene):polystyrene sulfonate (PEDOT:PSS) thin films (thickness, <1 μm) at the proper finger positions of the soft body frame (PDMS; thickness, ~200 μm) (Fig. 4A, left and middle left). The reason for the choice of this type of soft actuators was due to the low-voltage operation and thin, compact design. On the basis of the Joule heating–induced operation mechanism and proper design (*46*), this PEDOT:PSS/PDMS soft bilayer actuator exhibited a modest response time (~2 s) and bending deformation with increasing applied voltages (0 to 15 V) (Fig. 4, B and C, and fig. S17). In what follows, we integrated the activating e-skin into the soft body architecture (palm area) through a simple lamination process (Fig. 4A, middle right). At the same time, the controlling e-skin was also embedded into the human body (refer to Fig. 1C). For activation, separate power sources were applied to the e-skin (3.6 V) and actuators (15 to 20 V) (Fig. 4A, right). In this robotic design, we used the same base material (PDMS) for the body frame, actuators, and driving system so that every robot part could organically share the robot's soft response.

The e-skin–mediated wireless activation and corresponding wireless four-state manipulation of the soft robotic hand were visualized by thermographic imaging (Fig. 4D and movie S1). Considering that the bypassed electric current generated Joule heat throughout the entirety of the e-skins (even fine interconnects) and actuators, the mapping images showed what appeared to be the operating controlling e-skin (Fig. 4D, top) and the activated soft robotic hand (Fig. 4D, bottom). We found that the state of pressure sensing was discriminated by the movement of hotspots (resistor regions, highlighted as yellow circular lines) as a result of the accurate recognition of inputs (Fig. 4D, top). In addition, specific regions near the RF transmitter/receiver module were notably heated as the "heart" of the e-skins, validating the wireless inter-skin communication. When receiving the modulated signals and decoding them (refer to Fig. 3, C to G), the embedded activating e-skin started to activate the soft robotic hand with the capability of creating four-state motions matched to the input types in the controlling e-skin (Fig. 4D, bottom, and movie S2). A set of motion states and the bending curvature of the robotic fingers were easily controllable by the strategy of mixing digital output signals (fig. S14) and changing the bias voltage of the soft actuators

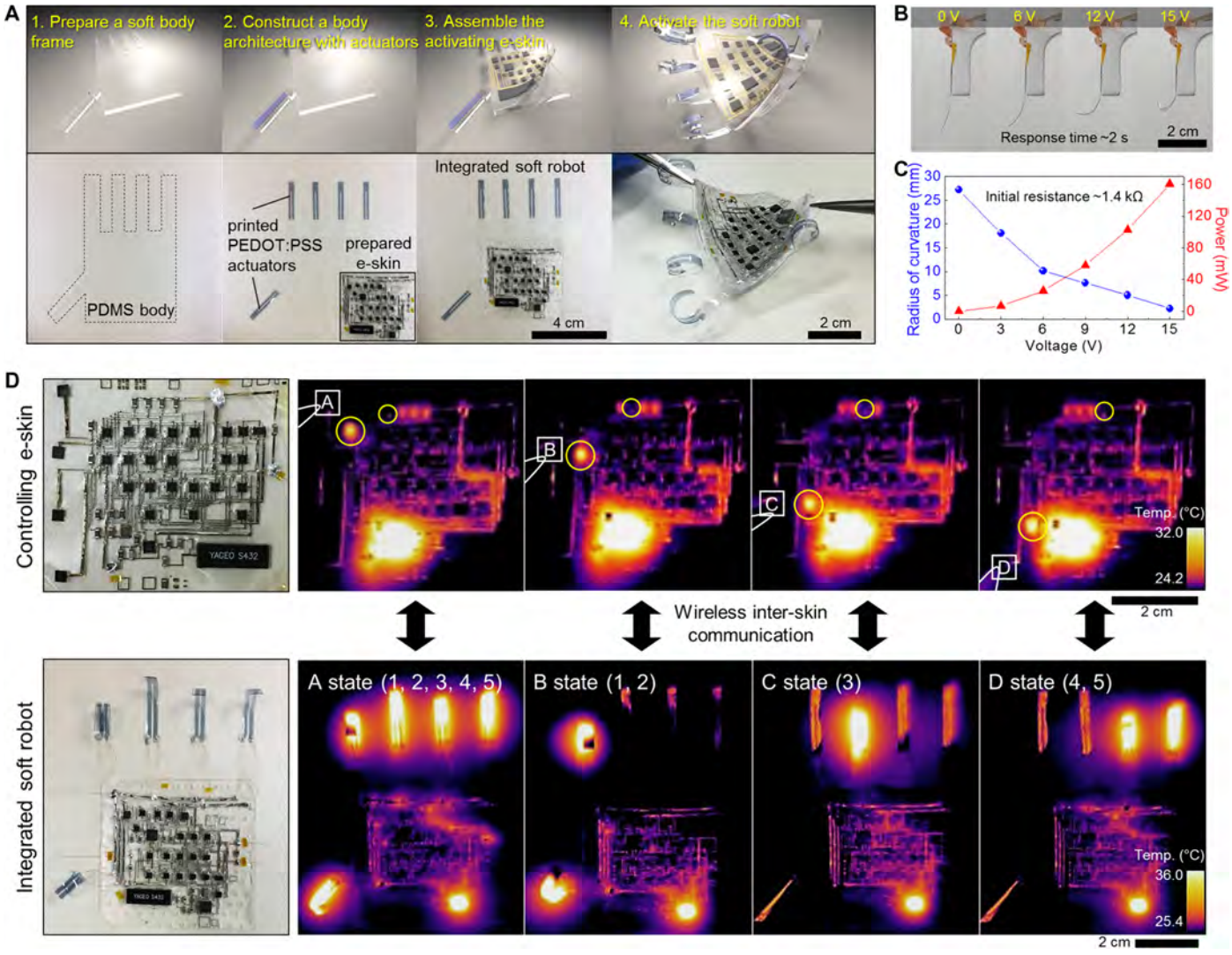

Fig. 4. E-skin–mediated assembly and wireless activation of a soft robotic hand. (**A**) Schematic and corresponding photographic images of soft, compact assembly steps for the integrated design of a fully soft robotic hand. A body architecture of the robot was fabricated by printing PEDOT:PSS thin films at finger positions. By using the prepared activating e-skin, the integration and activation process was carried out through a simple lamination process. (**B**) Sequential actuation profiles of an individual bilayer (PEDOT:PSS/PDMS) soft actuator with increasing applied voltages (0 to 15 V). (**C**) Radius of curvature and power consumption of an individual soft actuator as a function of the applied voltage (0 to 15 V). (**D**) Representative photographic and thermographic images of the operating e-skin pair and corresponding four-state manipulation of the soft robotic hand: the operating controlling e-skin (top) and activated soft robotic hand (bottom). On the basis of the specific digital mixing (fig. S14), each input state is programmed to activate different robotic fingers (A, "1, 2, 3, 4, 5"; B, "1, 2"; C, "3"; D, "4, 5"). According to the operational state of robotic fingers, in-skin current distribution was discriminated.

(Fig. 4, B and C). In each motion state, the involved current flow distribution varied according to which finger was operated, as if actual movements of human fingers were controlled by the operation of involved motor neurons (Fig. 4D, bottom).

Coadaptive movements of fully soft robotic design

The most salient feature of the fully soft design was the capability of coadaptive movements of a soft body architecture and embedded e-skin under multidimensional deformations. As described in Fig. 2 (C and D) and fig. S11, the fragmented design and corresponding minimized inherent hardness allowed the e-skin to conform to finely deformed and dynamic surfaces. On the basis of this feature, we showed that the e-skin–integrated soft robot could be actuated and mechanically deformed in ways not previously possible: A body architecture and embedded soft driving system could equally share the sequential deformation profiles such as outward (Fig. 5A) and inward bending (Fig. 5B), stretching (~20% diagonal strain) (Fig. 5C), folding (Fig. 5D), and harsh crumpling (fig. S18). This property is invaluable for a robot that frequently encounters highly restricted spaces with specific cross sections that are much smaller than the robot size (Fig. 5E). In this regard, we demonstrated sequential coadaptive movements that allowed the robot to pass through a tiny cross section at a folded state (Fig. 5F) and then operate with full motion states at an unfolded state inside the target space (Fig. 5G). For an experimental setup, we prepared a plastic bottle whose entrance diameter (33 mm) was smaller than the robot size (62 mm) (Fig. 5E). To obtain precise thermographic images of robot

operation without reflection or distortion, we cut away the top part of the bottle. From the successive thermographic image frames, we verified that the embedded e-skin in conjunction with the wireless inter-skin communication reliably controlled the robot throughout the entire flow of deformation steps: Four-state motion was equally conducted in confined places (Fig. 5H and movie S3).

Universal soft robotic activation based on reversible assembly

The presented concept of the two-part soft driving system is not only an attractive source for a fully soft robotic design but also a universal soft platform that can activate multiple types of electrically driven soft robots. In virtue of their softness and capability of wireless inter-skin communication, the single e-skin pair can consecutively trigger the e-skin–mediated wireless activation in various soft robots through repeatable lamination, regardless of their body architectures and deformation states. Figure 6A shows a conceptual experimental design of this concept. We prepared three different soft robotic hands with distinct finger designs (spread finger design for robots 2 and 3) and deformation states (curvilinear surface for robot 3) (Fig. 6B). The operating characteristics (bending curvature and power consumption) of each robot were similar to those depicted in Fig. 4C. For ease of demonstration, the location of the controlling e-skin was fixed onto the wrist (Fig. 6C). On the basis of the wireless inter-skin communication about robot control signals, wireless, consecutive soft robotic activation was carried out through the sequential lamination of the activating e-skin.

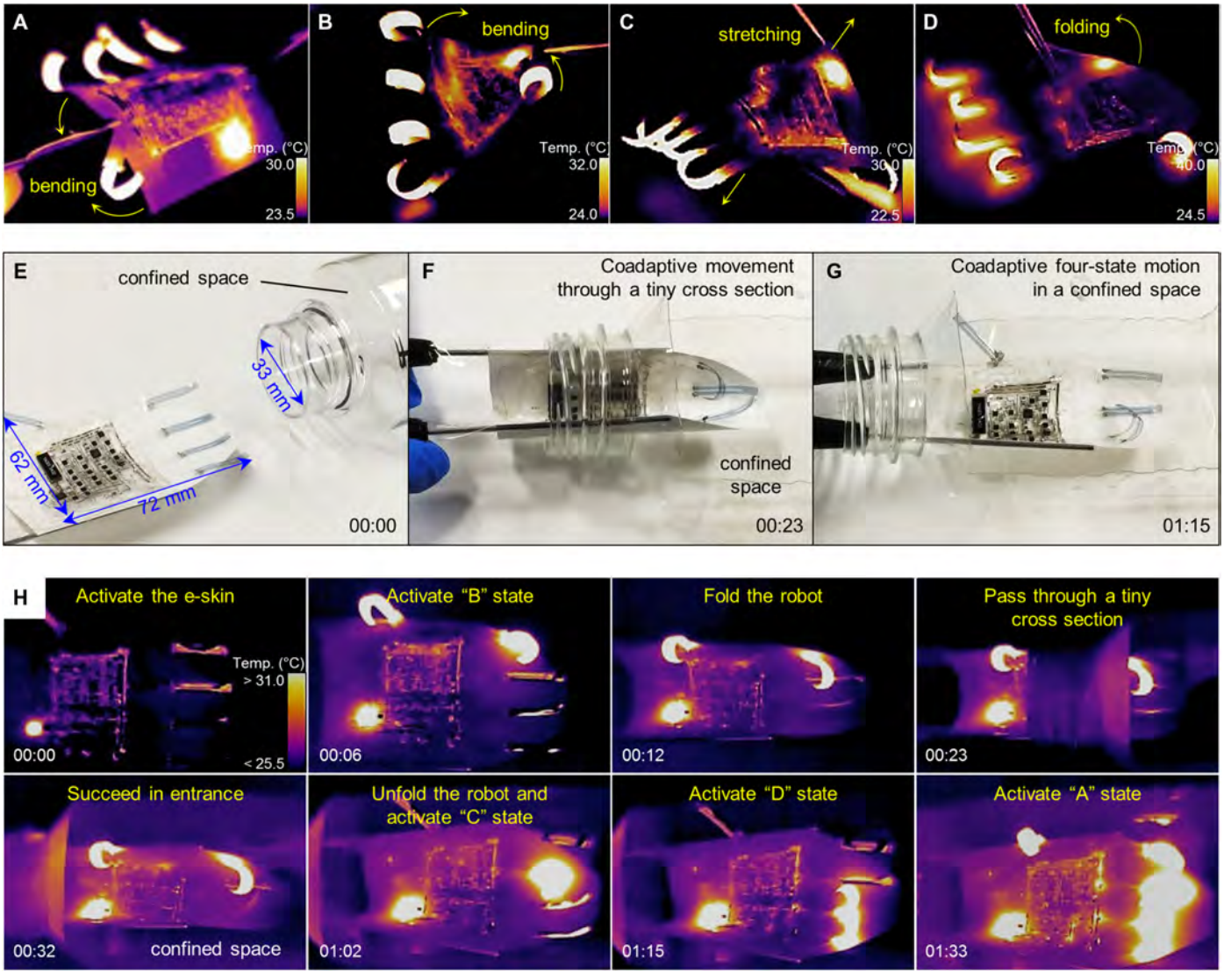

Fig. 5. Coadaptive movements of fully soft robotic design. (**A** to **D**) Thermographic images of the activated fully soft robot subject to multidimensional deformations such as outward (A) and inward bending (B), stretching (~20% diagonal strain) (C), and folding (D). Because of soft, thin, and lightweight features, the e-skin can equally share the sequential deformation profiles of the robot body. (**E**) Experimental design showing that the fully soft robot met the constrained environment, whose cross section (33 mm) was smaller than the robot size (62 mm). (**F** and **G**) Sequential coadaptive movements allow the robot to pass through a tiny cross section at a folded state (F) and then operate with full motion states at an unfolded state (G). (**H**) Sequential thermographic image frames that verify successful coadaptive movements and reliable operation of the robot throughout the entire flow of deformation steps.

Different actuation states (C, D, and B states as described in Fig. 4D) were adopted for each robot specifically for distinction between operations (Fig. 6, D and E, and movie S4). Because the actuating mechanism of every robot was analogous, the embedded e-skin pair could universally drive the soft robots. Further, the potential of this strategy could be easily extended to other robot functions or even the capability of multi-robot activation provided that body frames or circuit architectures of e-skins are reconfigured.

DISCUSSION

Soft robots with inherent hardness, mostly caused by driving parts, generally suffer weight, volume, and adaptability issues in constrained spaces. The results presented here establish a pathway for realizing fully soft robotic design based on a concept of soft electronics. We demonstrated a skin-like, two-part, soft driving system whose physical layout and electronic functionality were designed to show the maximum potential of fully soft robots activated by the e-skin. The physical design of this e-skin pair in terms of softness, thickness, weight, and fragmented SHE configuration realized soft, compact, reversible integration into many types of soft body architecture. We explored how this embedded e-skin pair constructed a reliable wireless interface between physically and electrically isolated soft bodies (such as human and a robot) and how this dynamic inter-skin communication could lead to the e-skin–mediated soft robotic activation. The resulting robotic design was highly compact and revealed that dynamic deformation profiles of the robot could be equally shared with every robot part without incurring any dislocations or interfacial failure. Further, we

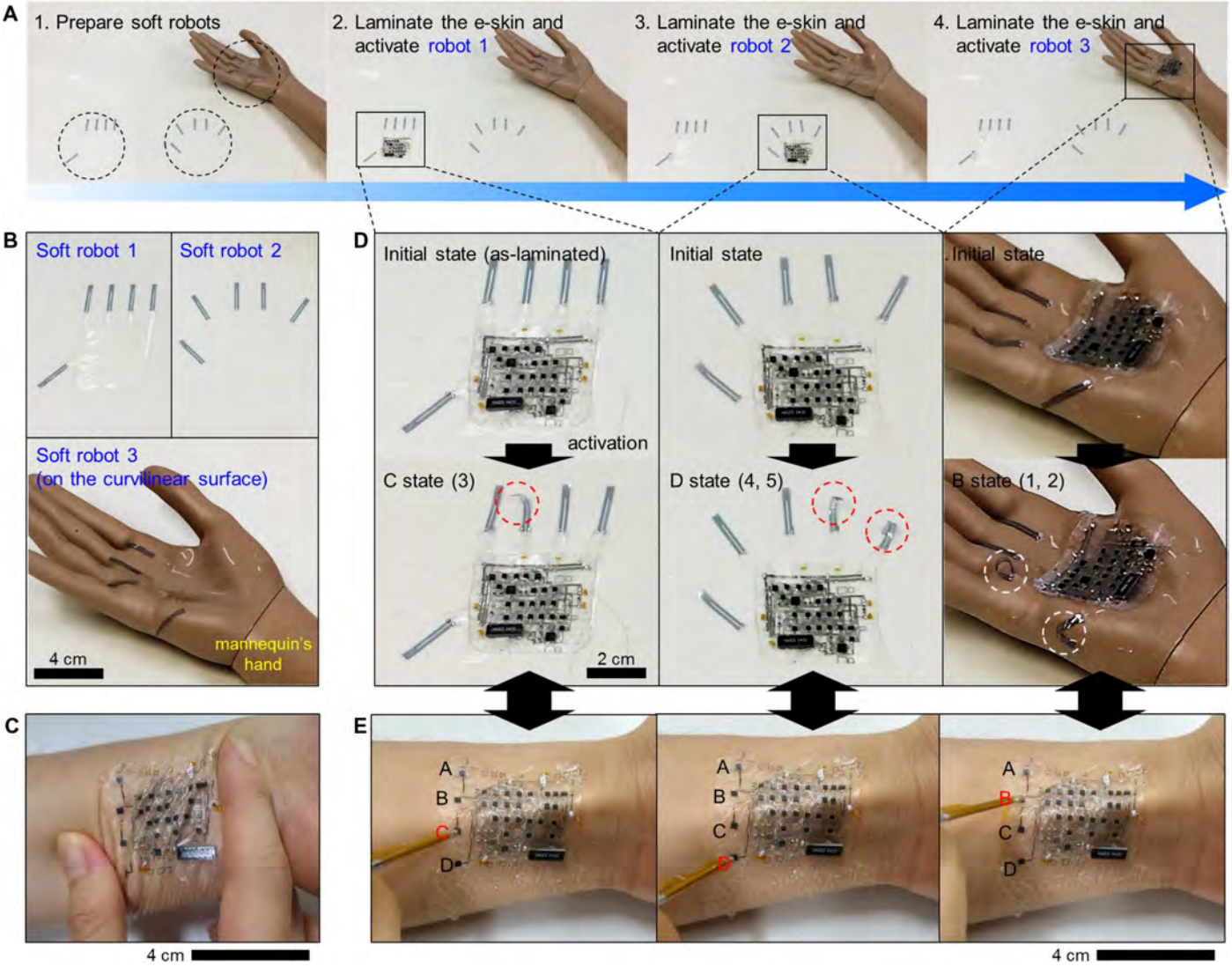

Fig. 6. Universal soft robotic activation based on reversible assembly. (**A**) Process flow of consecutive soft robotic activation by sequential lamination processes. Specifically, three different soft robotic hands with distinct finger designs (normal design for robot 1 and spread finger design for robots 2 and 3) and deformation states [placed onto the flat (robots 1 and 2) and curvilinear surface (robot 3) like a mannequin's hand] were addressed. (**B**) Enlarged view of each soft robotic hand before the activating e-skin was mounted. (**C**) Photograph of the laminated controlling e-skin showing good skin conformability. (**D**) Enlarged view of wireless manipulation of soft robotic hands with distinct operation states. For comparison, different actuation states in response to the input types (C, D, and B states) were demonstrated for each robot. (**E**) Sequential photographs of the controlling e-skin in each input state (C, D, and B).

verified that this type of soft driving system could be an attractive, universal platform for wireless robotic activation irrespective of the shape and deformation states of body frames.

In comparison with conventional soft robots that usually equip hard components in isolated spaces based on rigid assembly, the presented skin-type soft driving system and its way of soft assembly has potential for changing the paradigm of soft robotics in terms of how to softly and reversibly functionalize soft robots. On the basis of this approach, robot functions in future soft robotics need not be fixed but could be tunable only by replacing and/or reprogramming the driving e-skin. The unique compactness and integrated functionality of the skin-type driving system also prove the capability of extending the soft robot applications toward self-contained fully soft robots with highly compact design. In addition, our work helps pave the way for e-skin–mediated wireless interaction, either monitoring or communicating, between robots and human or other biological organisms.

MATERIALS AND METHODS

Surface-mountable devices

A total of 82 SMDs (49 IC devices, 31 passive components, and 2 antennas) were used to implement the e-skins. Given the system compactness and miniaturization, we used two-channel (two IC devices in a single SMD) SMDs. In particular, to minimize the inherent hardness of the e-skins, we mostly regulated the dimensions of assembled SMDs to smaller than 1.5 mm by 1.5 mm (see table S1 for specifications of all SMDs).

Design and fabrication of the e-skin pair

On the basis of the circuit diagrams depicted in fig. S1, we drew compact circuit layouts for both e-skins in the homemade circuit routing program (fig. S3). Several distinct contact pads were defined in proper regions for sensors, actuators, and power. Compared to our previous work (*34*, *35*), the role of rigid islands was replaced with printed extended epoxy architectures (figs. S7 to S9); hence, additional processes of loading the background image and pinpointing rigid islands for circuit design could be skipped. Salient information about printing pattern files and coordinate data of crossover lines and SMDs, necessary for subsequent continuous fabrication processes, was generated from the program by clicking the "Export" button (fig. S3C) (*34*). The fabrication of the designed circuit layouts began with preparing the prestrained PDMS (20:1 mixing ratio, Sylgard 184, Dow Corning) ($\varepsilon_x = \varepsilon_y = 30\%$). After 20 min of ultraviolet-ozone (UVO_3) (power = 29 mW cm^{-2}) treatment, Ag (ANP Corp.) interconnection networks were directly drawn on the basis of the designed configurations via an inkjet-printing process (DMP-2831 inkjet printer, Dimatix Corp.) and annealed at 125°C for 20 min. The conductivity of printed Ag interconnects was ~2×10^6 S m^{-1}, and the typical resistance was ~40 to 50 ohms cm^{-1} with 250-μm average line width. In the following step, thin PDMS (20:1 mixing ratio) patterns were printed by using a pneumatic control nozzle-jet printer (SHOTmini 200Sx, Musashi Engineering Inc.) at line-crossing positions and cured at 90°C for 120 min (fig. S5, A and B). Before fabricating Ag crossover lines, we printed two kinds of epoxy (Ag epoxy and pure epoxy) to form electrical contacts and strain-isolating structures matched to the contact pad configurations of each SMD. Upon the as-printed epoxy layers, various types of SMDs were picked and placed (specfic positions were obtained from the extracted coordinate data), and the epoxies were cured at 170°C for 60 min to form robust bonding. Subsequently, numerous sets of crossover lines were quickly defined by an inkjet-printing process with an additional 20 min of UVO_3 treatment process. After all SMDs and interconnects were fully integrated, releasing the prestrain generated 2D wrinkles over the whole surface, including Ag interconnects and PDMS surface (fig. S6), following the predistributed strain field that caused fading wrinkles near the contact areas due to the printed strain-isolating structures (fig. S8, C and D). Particularly for the controlling e-skin, four pressure sensors (2 mm by 2 mm by 0.2 mm; Velostat, Adafruit) were attached to the predefined contact pads with a small amount of PDMS. To improve the adhesion force, we last incorporated a soft, sticky adhesive layer (PS-2053, Polymer Science Inc.).

Electrical characterization of wireless inter-skin communication

All electrical signals were measured in the probe station under ambient conditions. To measure the modulated signals in both initial and stretched states (mainly 20 to 30% biaxial strain), we held the e-skins on the manually controllable stretching machine. While applying the power (3.6 V) to the e-skins, we put a probing tip into contact with the area of interest and measured the real-time signal flows by using an oscilloscope (DPO5104, Tektronix). Especially for analyzing a decoding process, we generated input signals whose encoded information (A to D) was randomly and rapidly (>40 Hz) varied by an FPGA board. The decoded 4-bit pulse sequences were simultaneously recorded using four different channels in the oscilloscope.

Fabrication of soft robotic hands

A soft robot body was prepared by cutting a thin PDMS (thickness, ~200 μm) into desired hand-like designs (Fig. 4A, left). After 30 min of UVO_3 treatment, PEDOT:PSS (Sigma-Aldrich) with 2 weight % of zonyl surfactant (Zonyl FS-300 fluoro-surfactant, ~40% solids in H_2O, Sigma-Aldrich) were inkjet-printed to form a thin-film bilayer soft actuator (Fig. 4A, middle left). Technically, the proper resistance (~1.3 to 1.8 kilohms) of the printed PEDOT:PSS thin films was obtained through a single-nozzle, five-pass sequential printing process without intermediate annealing processes. All printing processes were carried out at room temperature, and the as-printed actuators were annealed at 80°C for 30 min. For an integrated soft robot, the prepared activating e-skin was laminated onto the palm of the soft robotic hand, and then each actuator was connected to the predefined contact pads of the e-skin through copper wires (diameter, ~50 μm). For activation of the soft robotic hand, separate power sources were applied to the e-skin (3.6 V) and actuators (15 to 20 V).

Thermographic visualization of operating e-skins and soft robotic hands

Electric current flows throughout the entirety of the e-skins, and soft robotic hands were indirectly visualized in terms of Joule heating ($P = V^2/R$). On the basis of the specific setting conditions (emissivity = 0.86, reflected temperature = 24°C, ambient temperature = 24°C, and humidity = 19%), thermographic images of the system were captured by a thermal imaging camera (T420, FLIR).

SUPPLEMENTARY MATERIALS

robotics.sciencemag.org/cgi/content/full/3/18/eaas9020/DC1

Note S1. Fully printable SHE assembly and its physical properties.

Note S2. Design criteria of fragmented SHE design for fine conformability to soft robots.

Note S3. Details on wireless inter-skin communication flow.
Note S4. Details on experimental setup for the reliability test under artificial noise condition.
Fig. S1. Schematic circuit diagrams of the devised e-skin pair.
Fig. S2. SMD-level fragmentation of electronic functionalities.
Fig. S3. Circuit designs based on the homemade circuit routing program.
Fig. S4. Fully printable SMD assembly for e-skins.
Fig. S5. Multilayer interconnection design in e-skins.
Fig. S6. Two-dimensional wrinkled morphologies of an e-skin surface.
Fig. S7. Comparison between printed strain-isolating structures.
Fig. S8. Experimental verification of the gradual strain-absorbing effect near the SMD contact areas.
Fig. S9. Three-dimensional finite element analysis on printed coplanar strain-isolating architectures.
Fig. S10. Design criteria of fragmented SHE design for fine conformability.
Fig. S11. Stretchability and conformability to dynamic surfaces.
Fig. S12. Signal quantizing module in the controlling e-skin.
Fig. S13. Continuous monitoring of wireless inter-skin communication.
Fig. S14. Digital mixing of decoded signals in the activating e-skin.
Fig. S15. An experimental setup for the reliability test.
Fig. S16. Details on experimental setup for the reliability test of encoded and nonencoded signals under artificial noise condition.
Fig. S17. Bending force of the PEDOT:PSS soft actuator.
Fig. S18. Coadaptive movement of the e-skin–integrated soft robot laminated onto a crumpled convex surface.
Table S1. Specifications of the used SMDs.
Movie S1. Thermographic visualization of real-time activation of a soft robotic hand.
Movie S2. Wireless operation of the e-skin–integrated soft robotic hand via wireless inter-skin communication.
Movie S3. Coadaptive movement of a fully soft robotic hand in a confined space.
Movie S4. E-skin–mediated universal soft robotic activation.

REFERENCES AND NOTES

1. D. Rus, M. T. Tolley, Design, fabrication and control of soft robots. *Nature* **521**, 467–475 (2015).
2. C. Laschi, B. Mazzolai, M. Cianchetti, Soft robotics: Technologies and systems pushing the boundaries of robot abilities. *Sci. Robot.* **1**, eaa3690 (2016).
3. H. Zhao, K. O'Brien, S. Li, R. F. Shepherd, Optoelectronically innervated soft prosthetic hand via stretchable optical waveguides. *Sci. Robot.* **1**, eaai7529 (2016).
4. D. Trivedi, C. D. Rahn, W. M. Kier, I. D. Walker, Soft robotics: Biological inspiration, state of the art, and future research. *Appl. Bionics Biomech.* **5**, 99–117 (2008).
5. E. W. Hawkes, L. H. Blumenschein, J. D. Greer, A. M. Okamura, A soft robot that navigates its environment through growth. *Sci. Robot.* **2**, eaan3028 (2017).
6. A. Ramezani, S.-J. Chung, S. Hutchinson, A biomimetic robotic platform to study flight specializations of bats. *Sci. Robot.* **2**, eaal2505 (2017).
7. A. D. Marchese, D. D. Onal, D. Rus, Autonomous soft robotic fish capable of escape maneuvers using fluidic elastomer actuators. *Soft Robot.* **1**, 75–87 (2014).
8. T. Li, G. Li, Y. Liang, T. Cheng, J. Dai, X. Yang, B. Liu, Z. Zeng, Z. Huang, Y. Luo, T. Xie, W. Yang, Fast-moving soft electronic fish. *Sci. Adv.* **3**, e1602045 (2017).
9. Y. Wang, X. Yang, Y. Chen, D. K. Walnwright, C. P. Kenaley, Z. Gong, Z. Liu, H. Liu, J. Guan, T. Wang, J. C. Weaver, R. J. Wood, L. Wen. A biorobotic adhesive disc for underwater hitchhiking inspired by the remora suckerfish. *Sci. Robot.* **2**, eaan8072 (2017).
10. P. Polygerinos, Z. Wang, K. C. Galloway, R. J. Wood, C. J. Walsh, Soft robotic glove for combined assistance and at-home rehabilitation. *Robot. Auton. Syst.* **73**, 135–143 (2015).
11. E. T. Roche, R. Wohlfarth, J. T. B. Overvelde, N. V. Vasilyev, F. A. Piula, D. J. Mooney, K. Bertoldi, C. J. Walsh, A bioinspired soft actuated material. *Adv. Mater.* **26**, 1200–1206 (2014).
12. M. Calisti, M. Giorelli, G. Levy, B. Mazzolai, B. Hochner, C. Laschi, P. Dario, An octopus-bioinspired solution to movement and manipulation for soft robots. *Bioinspir. Biomim.* **6**, 036002 (2011).
13. C. Laschi, M. Cianchetti, B. Mazzolai, L. Margheri, M. Follador, P. Dario, Soft robot arm inspired by the octopus. *Adv. Robot.* **26**, 709–727 (2012).
14. H.-T. Lin, G. G. Leisk, B. Trimmer, GoQBot: A caterpillar-inspired soft-bodied rolling robot. *Bioinspir. Biomim.* **6**, 026007 (2011).
15. A. D. Marchese, R. K. Katzschmann, D. Rus, A recipe for soft fluidic elastomer robots. *Soft Robot.* **2**, 7–25 (2015).
16. B. Mosadegh, P. Polygerinos, C. Keplinger, S. Wennstedt, R. F. Shepherd, U. Gupta, J. Shim, K. Bertoldi, C. J. Walsh, G. M. Whitesides, Pneumatic networks for soft robotics that actuate rapidly. *Adv. Funct. Mater.* **24**, 2163–2170 (2014).
17. D. Yang, B. Mosadegh, A. Ainla, B. Lee, F. Khashai, Z. Suo, K. Bertoldi, G. M. Whitesides, Buckling of elastomeric beams enables actuation of soft machines. *Adv. Mater.* **27**, 6323–6327 (2015).
18. K. Jung, J. C. Koo, J. Nam, Y. K. Lee, H. R. Choi, Artificial annelid robot driven by soft actuators. *Bioinspir. Biomim.* **2**, S42–S49 (2007).
19. S. Song, M. Sitti, Soft grippers using micro-fibrillar adhesives for transfer printing. *Adv. Mater.* **26**, 4901–4906 (2014)
20. M. Manti, T. Hassan, G. Passetti, N. D'elia, C. Laschi, M. Cianchetti, A bioinspired soft robotic gripper for adaptable and effective grasping. *Soft Robot.* **2**, 107–116 (2015).
21. J.-y. Nagase, S. Wakimoto, T. Satoh, N. Saga, K. Suzumori, Design of a variable-stiffness robotic hand using pneumatic soft rubber actuators. *Smart Mater. Struct.* **20**, 105015 (2011).
22. Y. She, C. Li, J. Cleary, H.-J. Su, Design and fabrication of a soft robotic hand with embedded actuators and sensors. *J. Mech. Robot.* **7**, 021007 (2015).
23. C. D. Onal, X. Chen, G. M. Whitesides, D. Rus, Soft mobile robots with on-board chemical pressure generation, in *Proceedings of the International Symposium on Robotics Research* (ISRR, 2011), pp. 1–16.
24. M. T. Tolley, R. F. Shepherd, B. Mosadegh, K. C. Galloway, M. Wehner, M. Karpelson, R. J. Wood, G. M. Whitesides, A resilient, untethered soft robot. *Soft Robot.* **1**, 213–223 (2014).
25. N. W. Bartlett, M. T. Tolley J. T. B. Overvelde, J. C. Weaver, B. Mosadegh, K. Bertoldi, G. M. Whitesides, R. J. Wood, A 3D-printed, functionally graded soft robot powered by combustion. *Science* **349**, 161–165 (2015).
26. M. Wehner, R. L. Truby, D. J. Fitzgerald, B. Mosadegh, G. M. Whitesides, J. A. Lewis, R. J. Wood, An integrated design and fabrication strategy for entirely soft, autonomous robots. *Nature* **536**, 451–455 (2016).
27. S.-J. Park, M. Gazzola, K. S. Park, S. Park, V. D. Santo, E. L. Blevins, J. U. Lind, P. H. Campbell, S. Dauth, A. K. Capulli, F. S. Pasqualini, S. Ahn, A. Cho, H. Yuan, B. M. Maoz, R. Vijaykumar, J.-W. Choi, K. Deisseroth, G. V. Lauder, L. Mahadevan, K. K. Parker. Phototactic guidance of a tissue-engineered soft-robotic ray. *Science* **353**, 158–162 (2016).
28. D.-H. Kim, R. Ghaffari, N. Lu, J. A. Rogers, Flexible and stretchable electronics for biointegrated devices. *Annu. Rev. Biomed. Eng.* **14**, 113–128 (2012).
29. M. L. Hammock, A. Chortos, B. C.-K. Tee, J. B.-H. Tok, Z. Bao, 25th Anniversary Article: The evolution of electronic skin (e-skin): A brief history, design considerations, and recent progress. *Adv. Mater.* **25**, 5997–6038 (2013).
30. A. Chortos, J. Liu, Z. Bao, Pursuing prosthetic electronic skin. *Nat. Mater.* **15**, 937–950 (2016).
31. D.-H. Kim, N. Lu, R. Ma, Y.-S. Kim, R.-H. Kim, S. Wang, J. Wu, S. M. Won, H. Tao, A. Islam, K. J. Yu, T.-. Kim, R. Chowdhury, M. Ying, L. Xu, M. Li, H.-J. Chung, H. Keum, M. McCormick, P. Liu, Y.-W. Zhang, F. G. Omenetto, Y. Huang, T. Coleman, J. A. Rogers, Epidermal electronics. *Science* **333**, 838–843 (2011).
32. D. J. Lipomi, M. Vosgueritchian, B. C.-K. Tee, S. L. Hellstrom, J. A. Lee, C. H. Fox, Z. Bao, Skin-like pressure and strain sensors based on transparent elastic films of carbon nanotubes. *Nat. Nanotechnol.* **6**, 788–792 (2011).
33. B. C.-K. Tee, A. Chortos, A. Berndt, A. K. Nguyen, A. Tom, A. McGuire, Z. C. Lin, K. Tien, W.-G. Bae, H. Wang, P. Mei, H.-H. Chou, B. Cui, K. Deisseroth, T. N. Ng, Z. Bao, A skin-inspired organic digital mechanoreceptor. *Science* **350**, 313–316 (2015).
34. J. Byun, B. Lee, E. Oh, H. Kim, S. Kim, S. Lee, Y. Hong, Fully printable, strain-engineered electronic wrap for customizable soft electronics. *Sci. Rep.* **7**, 45328 (2017).
35. J. Byun, E. Oh, B. Lee, S. Kim, S. Lee, Y. Hong, A single droplet-printed double-side universal soft electronic platform for highly integrated stretchable hybrid electronics. *Adv. Funct. Mater.* **27**, 1701912 (2017).
36. S. Xu, Y. Zhang, L. Jia, K. E. Mathewson, K.-I. Jang, J. Km, H. Fu, X. Huang, P. Chava, R. Wang, S. Bhole, L. Wang, Y. J. Na, Y. Guan, M. Flavin, Z. Han, Y. Huang, J. A. Rogers, Soft microfluidic assemblies of sensors, circuits, and radios for the skin. *Science* **344**, 70–74 (2014).
37. S. Lin, J. Xu, X. Zhi, D. Chen, J. Miao, P. B. Shull, D. Cui, Design and fabrication of a stretchable circuit board for wireless posture measurement. *IEEE Electron Device Lett.* **38**, 399–402 (2017).
38. K.-I. Jang, K. Li, H. U. Chung, S. Xu, H. N. Jung, Y. Yang, J. W. Kwak, H. H. Jung, J. Song, C. Yang, A. Wang, Z. Liu, J. Y. Lee, B. H. Kim, J.-H. Kim, J. Lee, Y. Yu, B. J. Kim, H. Jang, K. J. Yu, J. Kim, Y. W. Lee, J.-W. Jeong, Y. M. Song, Y. Huang, Y. Zhang, J. A. Rogers, Self-assembled three dimensional network designs for soft electronics. *Nat. Commun.* **8**, 15894 (2017).
39. A. D. Valentine, T. A. Busbee, J. W. Boley, J. R. Raney, A. Chortos, A. Kotikian, J. D. Berrigan, M. F. Durstock, J. A. Lewis, Hybrid 3D printing of soft electronics. *Adv. Mater.* **29**, 1703817 (2017).
40. N. Lu, D.-H. Kim, Flexible and stretchable electronics paving the way for soft robotics. *Soft Robot.* **1**, 53–62 (2014).
41. M. D. Bartlett, E. J. Markvicka, C. Majidi, Rapid fabrication of soft, multilayered electronics for wearable biomonitoring. *Adv. Funct. Mater.* **26**, 8496–8504 (2017).

42. D. Wirthl, R. Pichler, M. Drack, G. Kettlguber, R. Moser, R. Gerstmayr, F. Hartmann, E. Bradt, R. Kaltseis, C. M. Siket, S. E. Schausberger, S. Hild, S. Bauer, M. Kaltenbrunner, Instant tough bonding of hydrogels for soft machines and electronics. *Sci. Adv.* **3**, e1700053 (2017).
43. F. Xiong, *Digital Modulation Techniques* (Artech House, 2000).
44. T. Arabi, J. Jones, G. Taylor, D. Riendeau, Modeling, simulation, and design methodology of the interconnect and packaging of an ultra-high speed source synchronous bus, in *Proceedings of the 7th IEEE Topical Meeting on Electrical Performance of Electronic Packaging* (IEEE, 1998), pp. 8–11.
45. M. A. M. Vieira, C. N. Coelho, D. C. da Silva, J. M. da Mata, Survey on wireless sensor network devices, in *Proceedings of the 9th IEEE International Conference on Emerging Technologies and Factory Automation* (IEEE, 2003), pp. 537–544.
46. S. Taccola, F. Greco, E. Sinibaldi, A. Mondini, B. Mazzolai, V. Mattoli, Toward a new generation of electrically controllable hygromorhpic soft actuators. *Adv. Mater.* **27**, 1668–1675 (2015).

Acknowledgments: We thank D.-Y. Lee for the helpful discussion and J. R. Song for help in designing schematic illustration. **Funding:** This work was supported by a National Research Foundation of Korea (NRF) grant funded by the Korean Government [Ministry of Science, ICT and Future Planning (MSIP)] (NRF-2016R1A5A1938472), the Center for Advanced Soft Electronics funded by the MSIP as Global Frontier Project (CASE-2015M3A6A5065309), and the Center for Integrated Smart Sensors, the Global Frontier Project by the MSIP (CISS-2016M3A6A6930050) for funding. S.C. and T.L. appreciate the financial support of the National Creative Research Laboratory program (Grant No. 2012026372) through the NRF, funded by the Korean Ministry of Science and ICT. **Author contributions:** J.B., Y.L., K.-J.C., J.K., and Y.H. conceived the experiments. J.B. and Y.L. designed and fabricated the e-skins and carried out most of the experiments. J.Y. fabricated PEDOT:PSS soft actuators. E.O., B.L., S.C., and T.L. assisted the circuit design, thermographic imaging, and finite element analysis. J.B., Y.L., K.-J.C., J.K., and Y.H. wrote the manuscript, and all authors discussed the results and commented on the manuscript. **Competing interests:** The authors declare that they have no competing interests. **Data and materials availability:** All data needed to evaluate the conclusions in the paper are present in the paper and/or the Supplementary Materials. Additional data related to this paper may be requested from the authors.

Submitted 3 January 2018
Accepted 20 April 2018
Published 30 May 2018
10.1126/scirobotics.aas9020

Citation: J. Byun, Y. Lee, J. Yoon, B. Lee, E. Oh, S. Chung, T. Lee, K.-J. Cho, J. Kim, Y. Hong, Electronic skins for soft, compact, reversible assembly of wirelessly activated fully soft robots. *Sci. Robot.* **3**, eaas9020 (2018).

Science Robotics

Electronic skins for soft, compact, reversible assembly of wirelessly activated fully soft robots

Junghwan Byun, Yoontaek Lee, Jaeyoung Yoon, Byeongmoon Lee, Eunho Oh, Seungjun Chung, Takhee Lee, Kyu-Jin Cho, Jaeha Kim and Yongtaek Hong

Sci. Robotics **3**, eaas9020.
DOI: 10.1126/scirobotics.aas9020